Heart rate reduction with ivabradine promotes shear stress-dependent anti-inflammatory mechanisms in arteries[1]

Le Luong[1,2], Hayley Duckles[1,2], Torsten Schenkel[3], Marwa M. Mahmoud[1,2], Jordi L. Tremoleda[5], Marzena Wylezinska-Arridge[6], Majid Ali[7], Neil P. Bowden[1,2], Mari-Cruz Villa-Uriol[2], Kim Van der Heiden[8], Ruoyu Xing[8], Frank J. Gijsen[8], Jolanda J. Wentzel[8], Allan Lawrie[1,2], Shuang Feng[1,2], Nadine Arnold[1], Willy Gsell[9], Angela Lungu[1,2], Rodney Hose[1,2], Tim Spencer[4], Ian Halliday[4], Victoria Ridger[1,2], Paul C. Evans[1,2]

[1]Department of Infection, Immunity and Cardiovascular Disease and [2]INSIGNEO Institute for in silico Medicine, University of Sheffield, Sheffield, UK; [3]Department of Engineering & Mathematics and [4]Materials and Engineering Research Institute, Sheffield Hallam University, UK; [5]Trauma Sciences, Queen Mary University of London, UK; [6]MRC Clinical Sciences Centre, Imperial College London, UK; [7]Division of Cardiovascular and Diabetes Research, University of Leeds, UK; [8]Erasmus MC, Rotterdam, the Netherlands; [9]Maccine Pte Ltd, Department of Imaging, Singapore.

Running title: Pharmacological enhancement of shear stress

Address correspondence to:
Professor Paul Evans
Department of Cardiovascular Science
Faculty of Medicine, Dentistry & Health
University of Sheffield
Medical School
Beech Hill Road
Sheffield S10 2RX, UK

E-mail: paul.evans@sheffield.ac.uk
Tel +44 (0)114 271 2591
Fax +44(0)114 271 1863

Total word count: 6104

SUMMARY

Aims
Blood flow generates wall shear stress (WSS) which alters endothelial cell (EC) function. Low WSS promotes vascular inflammation and atherosclerosis whereas high uniform WSS is protective. Ivabradine decreases heart rate leading to altered hemodynamics. Besides its cardio-protective effects, ivabradine protects arteries from inflammation and atherosclerosis via unknown mechanisms. We hypothesised that ivabradine protects arteries by increasing WSS to reduce vascular inflammation.

Methods and Results
Hypercholesterolemic mice were treated with ivabradine for 7 weeks in drinking water or remained untreated as a control. En face immunostaining demonstrated that treatment with ivabradine reduced the expression of pro-inflammatory VCAM-1 ($p<0.01$) and enhanced the expression of anti-inflammatory eNOS ($p<0.01$) at the inner curvature of the aorta. We concluded that ivabradine alters EC physiology indirectly via modulation of flow because treatment with ivabradine had no effect in ligated carotid arteries in vivo, and did not influence the basal or TNFα-induced expression of inflammatory (VCAM-1, MCP-1) or protective (eNOS, HMOX1, KLF2, KLF4) genes in cultured EC. We therefore considered whether ivabradine can alter WSS which is a regulator of EC inflammatory activation. Computational fluid dynamics demonstrated that ivabradine treatment reduced heart rate by 20% and enhanced WSS in the aorta.

Conclusions
Ivabradine treatment altered hemodynamics in the murine aorta by increasing the magnitude of shear stress. This was accompanied by induction of eNOS and suppression of VCAM-1, whereas ivabradine did not alter EC that could not respond to flow. Thus ivabradine protects arteries by altering local mechanical conditions to trigger an anti-inflammatory response.

INTRODUCTION

Heart rate is an important risk factor and therapeutic target in cardiovascular disease[1-6]. Elevated heart rate was associated with poor cardiovascular outcome in patients with heart failure or acute myocardial infarction [1, 2]. Correspondingly, interventions that lowered resting heart rate led to protection from experimental atherogenesis [5, 6] and reduced infarct size and mortality rates in patients with acute myocardial infarction[3]. A beneficial effect of heart rate reduction on coronary artery disease was also demonstrated in clinical trials using ivabradine. This compound decreases heart rate by inhibiting the I_f current in the sinus node, without affecting blood pressure or systolic ventricular function. Ivabradine treatment improved prognosis in patients with chronic heart failure[7] and had anti-ischemic effects in patients with stable angina[8]. Moreover, ivabradine was associated with a reduction in coronary endpoints in coronary artery disease patients with left ventricular dysfunction and heart rate ≥70 bpm[9]. Despite this, a recent study found that ivabradine did not have beneficial effects in patients with stable coronary artery disease but without heart failure[10], suggesting that its vasculoprotective effects may be restricted to patients with heart failure. The mechanism for the protective effects of ivabradine has been studied using animal models[11-14]. The administration of ivabradine reduced experimental atherosclerosis in hyperlipidaemic murine[13] and rabbit models [14]. However, molecular targets of ivabradine have not been identified in vascular cells and the atheroprotective effects of ivabradine are not due to a lipid-lowering effect of ivabradine, since the drug had no effects on cholesterol levels[11-13]. Taken together, these experiments suggest that a direct effect of ivabradine on vessels is unlikely, and suggest that reduction of heart rate may be a primary mechanism of action of the drug.

Arteries are exposed to mechanical forces including mechanical wall stress (tangential, longitudinal or circumferential) and blood-flow induced wall shear stress (WSS) that play important roles in vascular homeostasis and disease. Indeed, although atherosclerosis is associated with systemic risk factors, such as hypercholesterolemia, it develops preferentially at branches and bends of the arterial tree that are exposed to complex patterns of blood flow[15]. Computational fluid dynamic (CFD) studies have demonstrated that the magnitude of WSS (time-averaged WSS (TAWSS) over the cardiac cycle) is lower at atherosclerosis-prone sites exposed to complex flow compared to regions that are protected[16,17]. Low WSS promotes atherosclerosis by inducing endothelial expression of inflammatory molecules (e.g. VCAM-1) that promote lesions[18-20], whereas high unidirectional WSS induces anti-inflammatory genes such as eNOS[21]. Although ivabradine is known to increase stroke volume and coronary perfusion[22], its effects on WSS have not been studied. Here we tested the hypothesis that ivabradine protects arteries by enhancing WSS which reduces inflammatory activation of arterial EC.

MATERIAL AND METHODS
Animals, surgery, ivabradine treatment and diet
All experiments conform to the guidelines laid out in the UK Animals Scientific Procedures Act (1986) and to the guidelines from Directive 2010/63/EU of the European Parliament on the protection of animals used for scientific purposes, and were performed under a project license from the UK Home Office. LDLR^{-/-} (low-density lipoprotein receptor–deficient) mice on a C57BL/6 genetic background were obtained commercially from Jackson laboratories and then bred in-house. All mice used in this study were male. Mice were housed under specific-pathogen free conditions. Where indicated, mice of 8 weeks of age were anaesthetized using a mixture of ketamine, xylazine and atropine prior to surgical exposure of the carotid arteries. The right carotid artery was ligated using cotton thread immediately proximal to the carotid bifurcation. Mice were allowed to recover for 1 week prior to experimentation. Some animals were treated with ivabradine either by i.v. injection (5 mg/kg) or in drinking water *ad libitum* (162 mg/L for 1 or 7 weeks). Alternatively, mice remained untreated as a control. Where indicated, normal chow diet was replaced at 10 weeks of age with Diet W; a cholate-free high-fat Western-type diet (Arieblok Diet W, 4021.06; Woerden, Netherlands) for 6 weeks. The Diet W (high-fat diet) consisted of (w/w) Cocoa butter (15%), cholesterol (0.25%), sucrose (40.5%), cornstarch (10%), corn oil (1%), cellulose (5.95%), casein (20%), 50% choline chloride (2%), methionine (0.2%) and mineral mixture (5.1%), total fat content (16%).

***En face* staining.** Animals were killed using pentobarbital (800 mg/kg by intraperitoneal injection). Endothelial expression of VCAM-1 or eNOS was determined by *en face* staining of the murine aorta as described[18,20]. Briefly, aortae were perfusion fixed and isolated prior to permeabilisation using 0.5% Triton X-100 (Sigma-Aldrich), and blocking with 20% goat serum for 2 h at room temperature. After washing with phosphate-buffered saline, the tissue was incubated with anti-VCAM-1 (EPR505; Novus Biologicals UK) or anti-eNOS (BD Bioscences) primary antibodies overnight at 4 °C. The tissue was then washed with PBS and incubated with goat anti-rabbit IgG antibody conjugated to AlexaFluor-568 (A11036; Invitrogen) for 2-3 h at room temperature followed by incubation with AlexFlour-488 labelled anti-CD31 antibody (102514; BioLegend) for 72-120 h at 4 °C. The tissue was incubated with TOPRO-3 to counterstain nuclei. To control for specific binding, tissues were incubated with irrelevant rabbit IgG antibodies and appropriate fluorescent secondary antibodies, or were incubated with secondary antibodies alone. The ascending aorta and arch were mounted and images of the EC monolayer were obtained using an inverted laser-scanning confocal microscopy (LSM 510 Meta inverted; Zeiss, Oberkochen, Germany). Protected (outer curvature) and susceptible (inner curvature) regions of the aortic arch were located using anatomical landmarks as described[20]. The mean expression levels of VCAM-1 and eNOS were determined by pooling mean fluorescence values from multiple cells (> 50 cells per field of view).

EC culture and exposure to shear stress. Human umbilical vein EC (HUVEC) were isolated using collagenase digestion and cultured. EC at passage 3-5 were cultured until confluent in 6 well plates and exposed to flow using an orbital shaking platform (PSU-10i; Grant Instruments) housed inside a cell culture incubator[23]. The radius of orbit of the orbital shaker was 10 mm and the rotation rate was set to 210 rpm. This system generated low shear stress (approximately 5 dyn/cm^2) with rapid variations in direction in the centre and high shear stress (approximately 15 dyn/cm^2) with relatively uniform direction at the periphery[23].

Comparative real time PCR. The levels of transcripts were assessed using quantitative real time PCR (qRT-PCR) as described[18,23] using gene-specific primers (Supplementary Table 1). Relative gene expression was calculated by comparing the number of thermal cycles that were necessary to generate threshold amounts of product. Fold changes

were calculated using the ΔΔCt method.

Vascular geometry and heart rate measurements
Heart rate and blood pressure were measured in conscious, restrained LDLR^{-/-} mice using a commercial automated system Visitech Systems, Apex, NC. In order to familiarize mice to this procedure, daily measurements were carried out for two weeks prior to experimentation. Mean blood pressure and heart rate values were generated by pooling data from 20 measurements.

CT angiography was carried out as described (Inveon, Siemens)[24]. Electrocardiogram gating was used to minimize movement artefacts caused by the movement of the heart and of the vessel during the cardiac cycle. Thus all images were acquired at the same time point of the cycle, the end of diastole, to avoid scanning during the dilation of the aorta during systole. Transthoracic echocardiography was carried out using a commercial system (Vevo 770® with a RMV707B scan head, Visual Sonics, Toronto, Canada) as described[25]. Briefly mice were anaesthetised with isoflurane via oxygen before being placed supine on a heated platform and covered to minimise heat loss. Maintenance Isoflurane (0.5-1.5%) with oxygen was delivered via a nose cone. Following depilation, Doppler pulse wave velocities were captured from peak flow in the ascending aorta. Data were averaged from 3-5 measurements per mouse.

Computational fluid dynamics (CFD)
The triangulated lumen surface was imported into ANSYS ICEM-CFD to generate a high quality hybrid tetrahedral mesh with prismatic boundary layer. The use of a prismatic layer of 4 cells allows for accurate representation of the WSS using a low overall cell count. Preliminary grid sensitivity studies using grid sizes from 80,000 to 500,000 cells showed that the results for WSS were grid insensitive within 2% for a grid size of approximately 200,000 cells while allowing for low simulation times of approximately 8 h on 2 cores of a 2.5GHz Intel i7 processor.

The unsteady Navier-Stokes equations were solved numerically using the finite volume method (FVM) in ANSYS FLUENT 14.5. The vessel geometry was assumed to be rigid. Blood was modelled as a Newtonian fluid with a dynamic viscosity of $\mu = 0.004\,Pa\,s$ (4 cP) and a density of $\rho = 1235\frac{kg}{m^3}$. Using a typical maximum flow speed at the aortic root $V = 1\frac{m}{s}$ and the hydraulic diameter of $D = 1.58\,mm$, the maximum Reynolds number is

$$Re = \frac{\rho V D}{\nu} = 488.$$

The flow was therefore modelled as laminar.

The aortic root cross section was extruded by 10 diameters to allow for development of the flow and prescription of a Dirichlet inlet boundary condition for the normal velocity as a plug profile at the extruded section. The time dependent mean velocity was digitized from the US Doppler images and a 3rd order Bezier approximation[26] was used to generate a second-order-smooth mean velocity curve.

At the exit of the aorta descendens and the branches a Neumann outlet boundary condition was used with a flow split of 70, 16, 8 and 6 percent for aorta descendens, innominate, common carotid and subclavian, respectively.

Numerical solutions were obtained using cell based higher with second order pressure, quadratic upwind momentum and second order implicit time discretization. Time step size was chosen as 1/400th or 1/600th of the cycle time for the control and ivabradine cases, respectively, maximum Courant numbers were below 8. In addition to the solution vector, three dimensional WSS data for the aorta and the defined ROI at the outer and

inner curvature were area-averaged during run time. From the time-dependent WSS, the time-averaged WSS at the wall was calculated:

$$\bar{\tau} = \frac{1}{N} \sum_N \tau_n$$

Statistics   Differences between samples were analysed using an unpaired or paired Student's t-test, one-way ANOVA with Bonferroni's adjustment, or two-way ANOVA with Sidak's multiple comparison test.

RESULTS
Ivabradine reduced inflammation of arterial EC.
We hypothesized that ivabradine protects rodent arteries by reducing inflammatory activation of EC. This was assessed using LDLR^{-/-} mice exposed to a high fat diet for 6 weeks, a regime that is known to generate hypercholesterolemia and inflammatory activation of aortic EC[27]. In the first instance, we investigated whether oral ivabradine can reduce heart rate in LDLR^{-/-} mice. Male LDLR^{-/-} mice were exposed to ivabradine in drinking water for 7 weeks or were exposed to untreated water as a control (Fig. 1A). The average consumption of water in ivabradine-treated and control groups was similar (4.85 versus 5.27 ml/day/animal, respectively) and it was calculated that treated animals consumed an average of 27 mg/kg ivabradine daily. Pressure cuff measurements revealed that treatment with ivabradine reduced heart rate by approximately 20% but did not influence systolic or diastolic blood pressure (Fig. 1B). Thus although ivabradine was administered to LDLR^{-/-} mice at doses significantly greater than those used clinically (0.25-0.33 mg/kg/day) it caused a reduction in heart rate that was proportional to that observed in ivabradine-treated patients[7-9].

We examined whether reduced heart rate in ivabradine-treated mice was associated with an altered inflammatory profile using *en face* staining to quantify endothelial expression of molecules with inflammatory (VCAM-1) or anti-inflammatory (eNOS) function. In untreated mice, VCAM-1 expression in EC was significantly higher at the inner compared to the outer curvature (Fig. 2, left panels), whereas eNOS expression was comparable at the inner and outer curvature (Fig. 3, left panels). Treatment with ivabradine significantly reduced VCAM-1 expression and simultaneously increased eNOS expression at both the inner and outer curvatures demonstrating that ivabradine reduced inflammation in aortic EC (Figs. 2 and 3, compare left and right panels). Thus we conclude that ivabradine exerts anti-inflammatory effects in the murine aorta by inducing eNOS and by suppressing VCAM-1.

Ivabradine did not have direct pharmacological effects on EC.
We wished to know whether ivabradine reduces vascular inflammation directly by pharmacological modification of EC or whether it acts indirectly by altering heart rate and hemodynamics. To address this, we exposed cultured HUVEC to ivabradine and determined the expression of inflammatory and anti-inflammatory genes. HUVEC were cultured under shear stress for 72 h using an orbiting 6-well plate system that generates low mean shear stress at the centre, and high mean shear stress at the periphery. They were simultaneously exposed to ivabradine at concentrations that mimic those detected in plasma in ivabradine-treated individuals (25-50 ng/ml)[28]. Some cultures were subsequently treated with the proinflammatory cytokine TNFα to determine the effect of ivabradine on inflammatory responsiveness. qRT-PCR revealed that the expression of the inflammatory effector molecules VCAM-1 and MCP-1 was enhanced in EC exposed to low compared to high WSS, and that anti-inflammatory eNOS, HMOX1, KLF2 and KLF4 displayed the opposite pattern (Fig. 4, compare treatments 1 and 7). The application of TNFα enhanced the expression of VCAM-1, MCP-1 and HMOX-1 but reduced the expression of KLF2, KLF4 (under low WSS only) and eNOS (under high WSS only) (Fig. 4, compare treatments 1, 4 and 7, 10). Notably, treatment of EC with ivabradine had no effect on the expression of VCAM-1, MCP-1, KLF2, KLF4, HMOX-1 or eNOS under high WSS (compare treatments 1, 2, 3) or low WSS (compare 7, 8, 9), and did not alter their modulation by TNFα (compare 4, 5, 6 and 10, 11, 12). Thus we conclude that ivabradine does not alter EC inflammatory or protective responses directly.

The potential ability of ivabradine to alter EC directly was also studied by ligating carotid arteries in LDLR^{-/-} mice so that EC were exposed to static conditions. After carotid artery ligation, mice were exposed to ivabradine for 7 weeks (in drinking water as above) or to

untreated water as a control. En face staining revealed that eNOS expression was negligible in ligated arteries of control- or ivabradine-treated animals (Supplementary Figure). This observation is consistent with previous reports that eNOS is shear-sensitive[21] and indicates that ivabradine does not induce eNOS expression in EC directly via a pharmacological effect. In summary, ivabradine had anti-inflammatory effects in the aorta which is exposed to flow but did not influence EC in cultured EC or cuffed arteries exposed to static conditions. Thus we conclude that ivabradine does not alter EC activation directly. Instead, our data are consistent with the hypothesis that ivabradine reduces inflammation of arteries by altering hemodynamics.

Heart rate reduction by ivabradine increased average wall shear stress.
Next, we tested the hypothesis that ivabradine protects atheroprone sites by increasing the magnitude of WSS. This was studied by CFD, which relies on accurate measurement of vascular geometries and blood flow velocities. WSS is sensitive to changes in vascular diameter since it is inversely proportional to the vessel radius cubed. Because of this we examined whether treatment of mice with ivabradine altered the geometry of the aorta. MRI revealed that exposure of mice to ivabradine for 7 weeks (in drinking water as above) did not influence the diameter of the aortic arch (1.7 +/- 0.04 mm versus 1.76 +/- 0.06 mm respectively, p>0.1; measured between the brachiocephalic and left common carotid artery). We next assessed the effects of ivabradine on blood flow velocities which were measured by transthoracic echocardiography. Since mice were anesthetised for this procedure, ivabradine was administered by intra-venous injection to ensure high precision in dose and timing. We wished to achieve a heart rate reduction of approximately 20% since this is similar to the reduction observed in mice used for assessment of inflammation (Fig. 1B). Using varying doses of ivabradine (0.5, 5 or 15 mg/kg) we observed that ivabradine reduced heart rate in a dose-dependent manner (Fig. 5A). Subsequent studies of the effects of ivabradine on blood flow were carried out using 5 mg/kg ivabradine because this dose achieved an approximate 20% reduction in heart rate (Fig. 5A). We observed that ivabradine treatment significantly altered blood flow velocity in the ascending aorta by enhancing both the peak velocity and the average velocity over the cardiac cycle (Fig. 5B). Unsteady CFD simulations were then performed using time-varying waveforms from ivabradine-treated versus control animals as inlet boundary conditions and a single representative geometry. The kinetic changes in WSS magnitude were determined over the cardiac cycle for anatomically-distinct portions of the aortic arch. At the inner curvature WSS displayed a transient peak followed by a rapid decline in magnitude (Fig. 5C). By contrast, WSS magnitude declined less rapidly following systole in the outer curvature and was therefore higher in the outer compared to the inner curvature for most of the cardiac cycle (Fig. 5C). Consistent with this, mapping of time-averaged WSS onto the geometry of the aortic arch revealed higher values at the outer compared to the inner curvature (Fig. 6, left panels) as described[16, 29, 30]. Treatment with ivabradine generated a prolonged higher flow rate in the aorta after systole leading to a prolonged higher level WSS (Fig. 5C) and thus an enhanced time-averaged WSS at both the inner and outer curvatures (Fig. 6, compare left and right panels). These data linking reduced EC inflammatory activation with enhancement in time-averaged WSS in response to ivabradine are consistent with the hypothesis that ivabradine reduces inflammation in the aortic arch by enhancing the magnitude of WSS.

DISCUSSION

Ivabradine treatment has been used successfully to treat coronary artery disease[8, 9] and can also reduce atherosclerosis in experimental models[11-13]. In particular, ivabradine prevented renal and cerebral endothelial dysfunction in a mouse transgenic model of mild dyslipidaemia[11] and prevented atherosclerotic lesion formation[13] and improved erectile function[12] in hypercholesterolemic ApoE^{-/-} mice. The underlying mechanism has remained elusive because ivabradine-targets have not been identified in vascular cells and ivabradine did not influence plasma lipid levels[11, 13]. Given that ivabradine alters heart rate, stroke volume and coronary perfusion[22], we tested the hypothesis that ivabradine may exert protective effects of arteries indirectly by altering hemodynamics which has been tightly linked to cardiovascular disease[15-17]. Our study demonstrated that ivabradine significantly altered flow in the murine aorta leading to enhanced WSS magnitude at both atheroprone and atheroprotected sites. Ivabradine induced protection from inflammation in the aorta (exposed to flow) but did not alter the inflammatory state of EC in conditions where flow was unaltered (either *in vitro* or *in vivo*), providing strong evidence that ivabradine functions indirectly via alteration of vascular mechanics. This is consistent with *in vitro* studies showing that VCAM-1 expression correlates inversely with shear stress magnitude[31].

Although it is well established that flow influences vascular function and disease, the relative contributions of WSS and mechanical wall stress remain uncertain. This is exemplified by Bolduc et al[32] who compared the effects of heart rate reduction with ivabradine or metoprolol (β blocker) on arterial physiology and plaque development in hypercholesterolemic mice. Although metoprolol and ivabradine had similar effects on heart rate reduction, the influence of these compounds on vascular physiology varied according to anatomical location. In cerebral arteries and the aorta, ivabradine restored function and reduced plaque more effectively than metoprolol indicating that its protective effects include factors other than heart rate reduction per se. We propose that ivabradine confers additional vasculoprotective effects by enhancing stroke volume leading to elevated WSS. On the other hand, Bolduc et al[32] found that ivabradine and metoprolol reduced carotid artery stiffness to a similar degree and suggested that this was due to reduced mechanical wall stress as a result of lowered heart rate. Collectively, these and our own observations suggest that ivabradine can modulate vascular function by altering mechanical stress as well as WSS and that the relative importance of these factors may vary according to anatomical site.

The effects of ivabradine on cardiovascular hemodynamics and physiology partially mimic protection afforded by physical exercise which can also lower resting pulse rate and enhance stroke volume[22]. In clinical studies, exercise at 140-180% above resting heart rate enhanced peak blood flow velocity and increased WSS in the aorta[33, 34]. Bolduc et al[32] compared the effects of ivabradine and physical exercise in hypercholesterolemic mice and found that while increased exercise and ivabradine both normalised cerebral artery function, only ivabradine reduced carotid artery stiffness. Further studies are required to determine whether the differential effects of these interventions on carotid and cerebral artery physiology are due to divergent effects on WSS and vascular mechanical stress.

The numerical model used is consistent with models used in previous studies[16, 29, 30]. Since WSS is inversely proportional to the cubed radius of the vessel, vascular remodelling in response to ivabradine could have major effects on WSS. However, while ivabradine treatment significantly enhanced arterial blood flow velocity it did not modify the geometry of the aorta. Because of these considerations we compared fluid dynamics of ivabradine-treated and control mice using distinct inlet velocities (boundary conditions) applied to a single representative geometry. An important simplification of the numerical model was the use of a rigid geometry. In a detailed study of the murine aorta, Trachet et

9

al[35] demonstrate that the inclusion of distensibility resulted in more realistic flow velocity waveforms using fluid structure interactions (FSI) compared to CFD using a rigid geometry. However, CFD and FSI gave similar predictions of WSS at proximal sites near the model inlet[35]. Because of this, we reason that the use of a rigid model in our simulations is justifiable because modelling is restricted to the aortic arch which is proximal to the flow inlet. Moreover, vascular distensibility may have relatively minor effects on WSS simulations in rodent vasculature since de Wilde demonstrated that CFD and FSI simulations were almost identical in murine carotid arteries[36]. Nevertheless, the use of a rigid geometry is a simplifying assumption that inevitably leads to a degree of error and prospective FSI studies should now be carried out to validate our observations using CFD. A second simplication concerns the physical properties of blood. Since blood is a highly concentrated suspension of red blood cells, it will exhibit non-Newtonian behaviour. However, since the level of shear rates in the murine aorta are relatively high, the assumption of Newtonian behaviour of blood is considered to be valid.

Our observation that ivabradine reduces arterial expression of VCAM-1 is consistent with its ability to protect against atherogenesis[11-13]. The mechanism may involve eNOS, which was induced by ivabradine in our study and is known to inhibit inflammation via NO-dependent nitrosylation of pro-inflammatory signalling intermediaries and transcription factors[21, 37]. Notably, previous studies revealed that high WSS enhanced the expression of eNOS and reduced VCAM-1[18-21]. Thus we hypothesize that ivabradine suppresses EC expression of VCAM-1 via WSS-dependent induction of eNOS. However, it is also plausible that the enhancement of WSS and/or modulation of vascular mechanical stress in response to ivabradine reduces inflammation via other mechanosensitive anti-inflammatory molecules including KLF2, Nrf2 and MKP-1[38, 39].

In summary, we have identified a pharmacological approach using ivabradine to elevate WSS in the arterial tree. Altered WSS in response to ivabradine was accompanied by induction of a mechanosensitive protective gene (eNOS) and suppression of inflammatory VCAM-1. These observations demonstrate that ivabradine protects arteries by altering local mechanical conditions including increased WSS magnitude which triggers an anti-inflammatory response. In addition to providing an explanation for the protective effects of ivabradine, our study has broader significance by suggesting that interventions that alter blood flow (e.g. heart rate reduction by ivabradine or exercise) protect the vasculature, in part, by modulating local WSS.

REFERENCES

1. Fox K, Borer JS, Camm AJ et al. Resting heart rate in cardiovascular disease. *J Am Coll Cardiol*. 2007;50:823-830.

2. Perski A, Olsson G, Landou C et al. Minimum heart-rate and coronary atherosclerosis - independent relations to global severity and rate of progression of angiographic lesions in men with myocardial-infarction at a young age. *Am Heart J*. 1992;123:609-616

3. Kjekshus JK. Importance of heart-rate in determining beta-blocker efficacy in acute and long-term acute myocardial-infarction intervention trials. *American J Cardiol*. 1986;57:F43-F49

4. Kaplan JR, Manuck SB, Clarkson TB. The influence of heart-rate on coronary-artery atherosclerosis. *J Cardiovasc Pharmacol*. 1987;10:S100-S103

5. Beere PA, Glagov S, Zarins CK. Experimental atherosclerosis at the carotid bifurcation of the cynomolgus monkey - localization, compensatory enlargement, and the sparing effect of lowered heart-rate. *Arterioscler Thromb*. 1992;12:1245-1253

6. Beere PA, Glagov S, Zarins CK. Retarding effect of lowered heart-rate on coronary atherosclerosis. *Science*. 1984;226:180-182

7. Swedberg K, Komajda M, Boehm M et al. Ivabradine and outcomes in chronic heart failure (shift): A randomised placebo-controlled study. *Lancet*. 2010;376:875-885

8. Tardif JC, Ford I, Tendera M et al, Initiative I. Efficacy of ivabradine, a new selective i-f inhibitor, compared with atenolol in patients with chronic stable angina. *Eur Heart J*. 2005;26:2529-2536

9. Fox K, Ford I, Steg PG et al Investigators B. Ivabradine for patients with stable coronary artery disease and left-ventricular systolic dysfunction (beautiful): A randomised, double-blind, placebo-controlled trial. *Lancet*. 2008;372:807-816

10. Fox K, Ford I, Steg PG et al. Ivabradine in stable coronary artery disease without clinical heart failure. *New Eng J Med*. 2014;371:1091-1099

11. Drouin A, Gendron ME, Thorin E et al. Chronic heart rate reduction by ivabradine prevents endothelial dysfunction in dyslipidaemic mice. *Brit J Pharmacol*. 2008;154:749-757

12. Baumhakel M, Custodis F, Schlimmer N, et al. Heart rate reduction with ivabradine improves erectile dysfunction in parallel to decrease in atherosclerotic plaque load in apoe-knockout mice. *Atherosclerosis*. 2010;212:55-62

13. Custodis F, Baumhaekel M, Schlimmer N, et al. Heart rate reduction by ivabradine reduces oxidative stress, improves endothelial function, and prevents atherosclerosis in apolipoprotein e-deficient mice. *Circulation*. 2008;117:2377-2387

14. Koniari I, Mavrilas D, Papadaki H, et al. Structural and biomechanical alterations in atherosclerotic thoracic aortas of hyperlipidemic rabbits treated with simvastatin and ivabradine. *Eur Heart J*. 2011;32:510-510

15. Kwak BR, Baeck M, Bochaton-Piallat ML, et al. Biomechanical factors in atherosclerosis: Mechanisms and clinical implications. *Eur Heart J*. 2014;35:3013-3020.

16. Suo J, Ferrara DE, Sorescu D et al. Hemodynamic shear stresses in mouse aortas: Implications for atherogenesis. *Arterioscler Thromb Vasc Biol*. 2007;27:346-351

17. Samady H, Eshtehardi P, McDaniel MC, et al. Coronary artery wall shear stress is associated with progression and transformation of atherosclerotic plaque and arterial remodeling in patients with coronary artery disease. *Circulation*. 2011;124:779-788

18. Cuhlmann S, Van der Heiden K, Saliba D, et al. Disturbed blood flow induces rela expression via c-jun n-terminal kinase 1 a novel mode of nf-kappa b regulation that promotes arterial inflammation. *Circ Res*. 2011;108:950-959

19. Chiu JJ, Lee PL, Chen CN, et al. Shear stress increases icam-1 and decreases vcam-1 and e-selectin expressions induced by tumor necrosis factor-alpha in endothelial cells. *Arterioscler Thromb Vasc Biol*. 2004;24:73-79

20. Iiyama K, Hajra L, Iiyama M, et al. Patterns of vascular cell adhesion molecule-1 and intercellular adhesion molecule-1 expression in rabbit and mouse atherosclerotic lesions and at sites predisposed to lesion formation. *Circ Res*. 1999;85:199-207

21. Cheng C, Haperen RV, Waard MD, et al. Shear stress affects the intracellular distribution of enos : Direct demonstration by a novel in vivo technique plenary paper shear stress affects the intracellular distribution of enos : Direct demonstration by a novel in vivo technique. *Blood*. 2005;106:3691-3698

22. Lauzier B, Vaillant F, Gelinas R et al. Ivabradine reduces heart rate while preserving metabolic fluxes and energy status of healthy normoxic working hearts. *Am J Physiol Heart Circ Physiol* 2011;300:H845-H852.

23. Warboys CM, de Luca A, Amini N, et al. Disturbed flow promotes endothelial senescence via a p53-dependent pathway. *Arterioscler Thromb Vasc Biol*. 2014;34:985-995

24. Van Doormaal MA, Kazakidi A, Wylezinska M, et al. Haemodynamics in the mouse aortic arch computed from mri-derived velocities at the aortic root. *J Roy Soc Int*. 2012;9:2834-2844

25. Hameed AG, Arnold ND, Chamberlain J, et al. Inhibition of tumor necrosis factor-related apoptosis-inducing ligand (trail) reverses experimental pulmonary hypertension. *J Exp Med* 2012;209:1919-1935

26. Schenkel T, Malve M, Reik M et al. Mri-based cfd analysis of flow in a human left ventricle: Methodology and application to a healthy heart. *Ann Biomed Eng*. 2009;37:503-515

27. Amini N, Boyle JJ, Moers B, et al. Requirement of jnk1 for endothelial cell injury in atherogenesis. *Atherosclerosis*. 2014;235:613-618

28. Feintuch A, Ruengsakulrach P, Lin A, et al. Hemodynamics in the mouse aortic arch as assessed by mri, ultrasound, and numerical modeling. *Am J Physiol. Heart Circ Physiol*. 2007;292:884-892

29. Ragueneau I, Laveille C, Jochemsen R, et al. Pharmacokinetic-pharmacodynamic modeling of the effects of ivabradine, a direct sinus node inhibitor, on heart rate in healthy volunteers. *Clin Pharmacol Ther*. 1998;64:192-203.

30. Huo Y, Guo X, Kassab GS. The flow field along the entire length of mouse aorta and primary branches. *Ann Biomed Eng*. 2008;36:685-699

31. Tsou JK, Gower RM, Ting HJ, et al. Spatial regulation of inflammation by human aortic endothelial cells in a linear gradient of shear stress. *Microcirculation (New York, N.Y. : 1994)*. 2008;15:311-323

32. Bolduc V, Drouin A, Gillis M-A, et al. Heart rate-associated mechanical stress impairs carotid but not cerebral artery compliance in dyslipidemic atherosclerotic mice. *Am J Physiol-Heart Circ Physiol*. 2011;301:H2081-H2092

33. Weber TF, von Tengg-Kobligk H, Kopp-Schneider A et al. High-resolution phase-contrast mri of aortic and pulmonary blood flow during rest and physical exercise using a mri compatible bicycle ergometer. *Eur J Radiol*. 2011;80:103-108

34. Suh G-Y, Les AS, Tenforde AS, et al. Hemodynamic changes quantified in abdominal aortic aneurysms with increasing exercise intensity using mr exercise imaging and image-based computational fluid dynamics. *Ann Biomed Eng*. 2011;39:2186-2202

35. Trachet B, Bols J, Degroote J et al. An animal-specific fsi model of the abdominal aorta in anesthetized mice. *Ann Biomed Eng*. 2015;43:1298-1309

36. David De Wilde. Wall shear stress metrics and their relation to atherosclerosis: an experimental and computational study in mice. Gent, Belgium. ISBN 978-90-8578-875-1

37. Natarajan R, Gupta S, Fisher BJ et al. Nitric oxide suppresses il-8 transcription by inhibiting c-jun n-terminal kinase-induced ap-1 activation. *Exp Cell Res*. 2001;266:203-212

38. Dekker RJ, van Soest S, Fontijn RD et al. Prolonged fluid shear stress induces a distinct set of endothelial cell genes, most specifically lung kruppel-like factor (klf2). *Blood*. 2002;100:1689-1698

39. Zakkar M, Chaudhury H, Sandvik G et al. Increased endothelial mitogen-activated protein kinase phosphatase-1 expression suppresses proinflammatory activation at sites that are resistant to atherosclerosis. *Circ Res*. 2008;103:726-732.
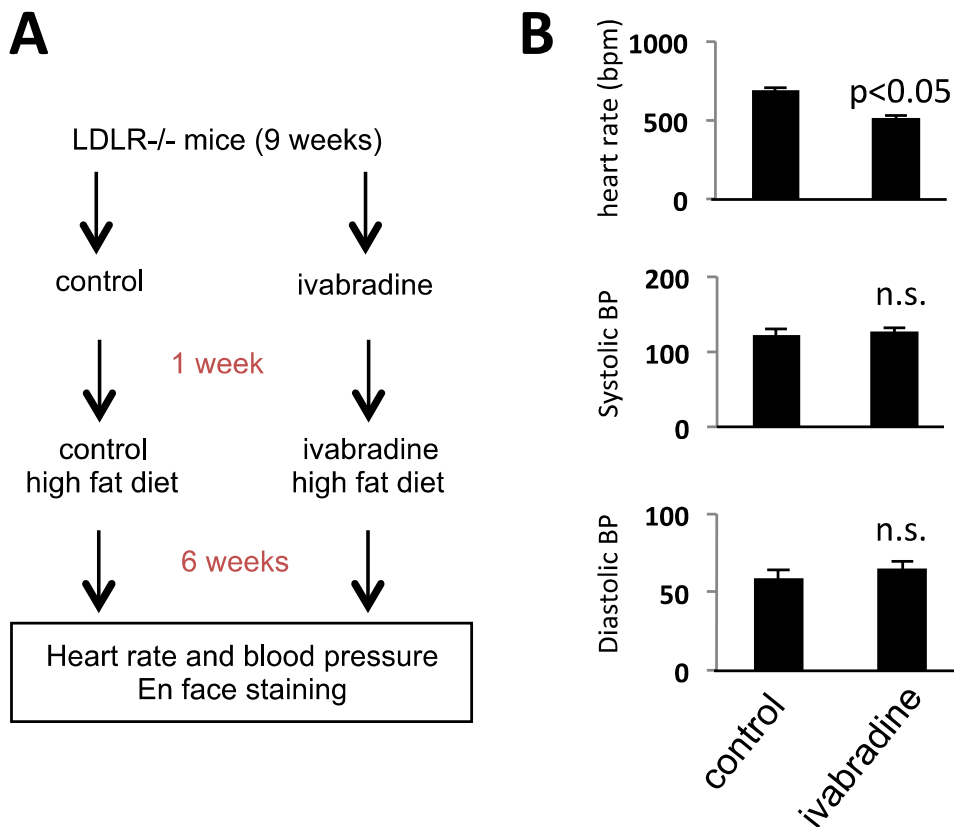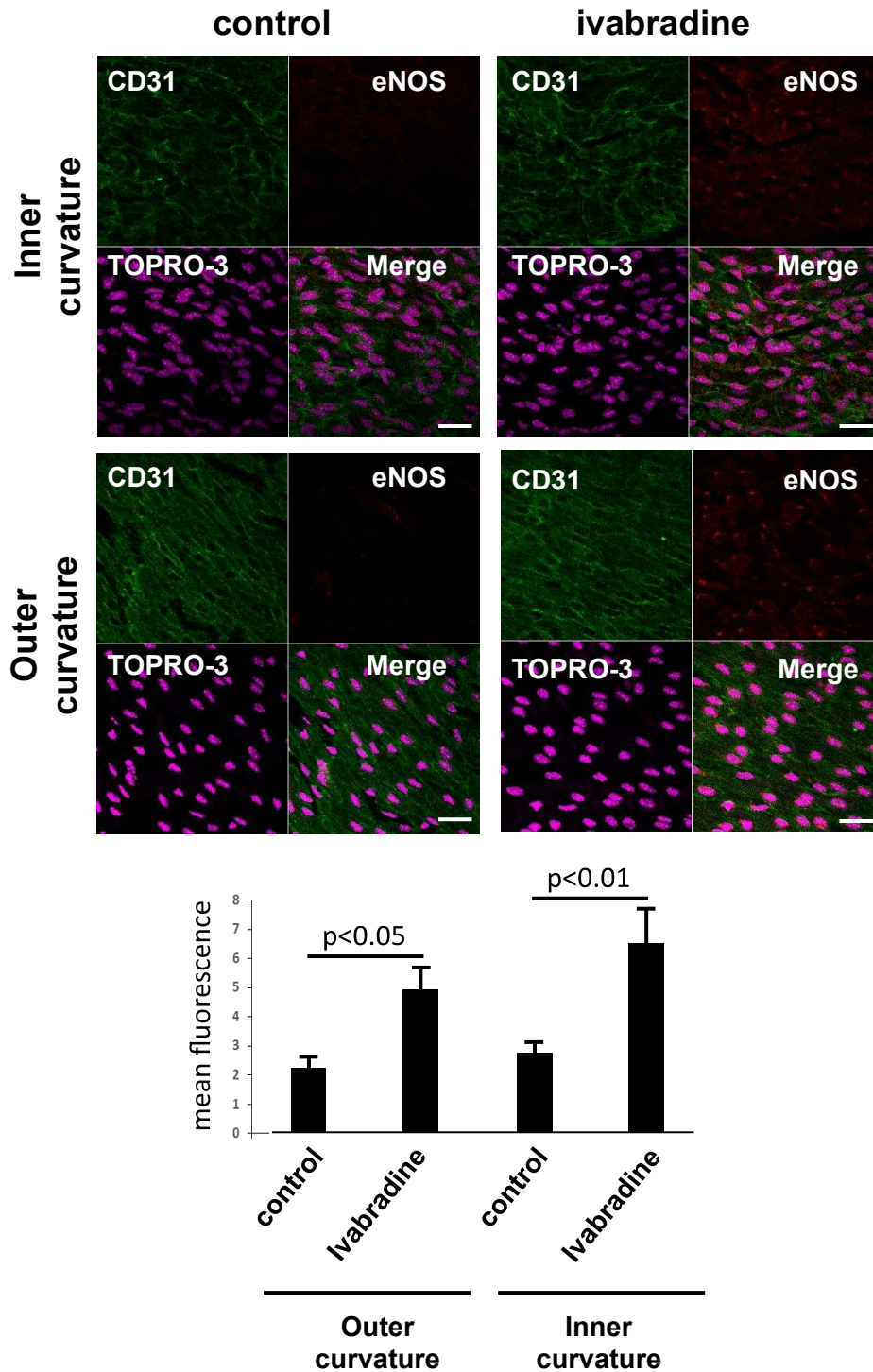
Figure 1 **Ivabradine treatment reduced heart rate in a murine model.** LDLR$^{-/-}$ mice aged 9 weeks were treated using ivabradine (in drinking water) or remained untreated as a control (n=5 per group). After 1 week, both groups of mice were exposed to a high fat diet in the presence of absence of ivabradine treatment. Following 6 weeks, heart rate and blood pressure measurements were made and EC expression of specific proteins was determined by en face staining. (A) An overview of the experimental approach is shown. (B) Mean heart rates (upper panel), systolic (centre panel) and diastolic blood pressures (lower panel) +/- standard deviations are shown. Differences between means were analysed using an unpaired Student's t-test. n.s., non-significant.
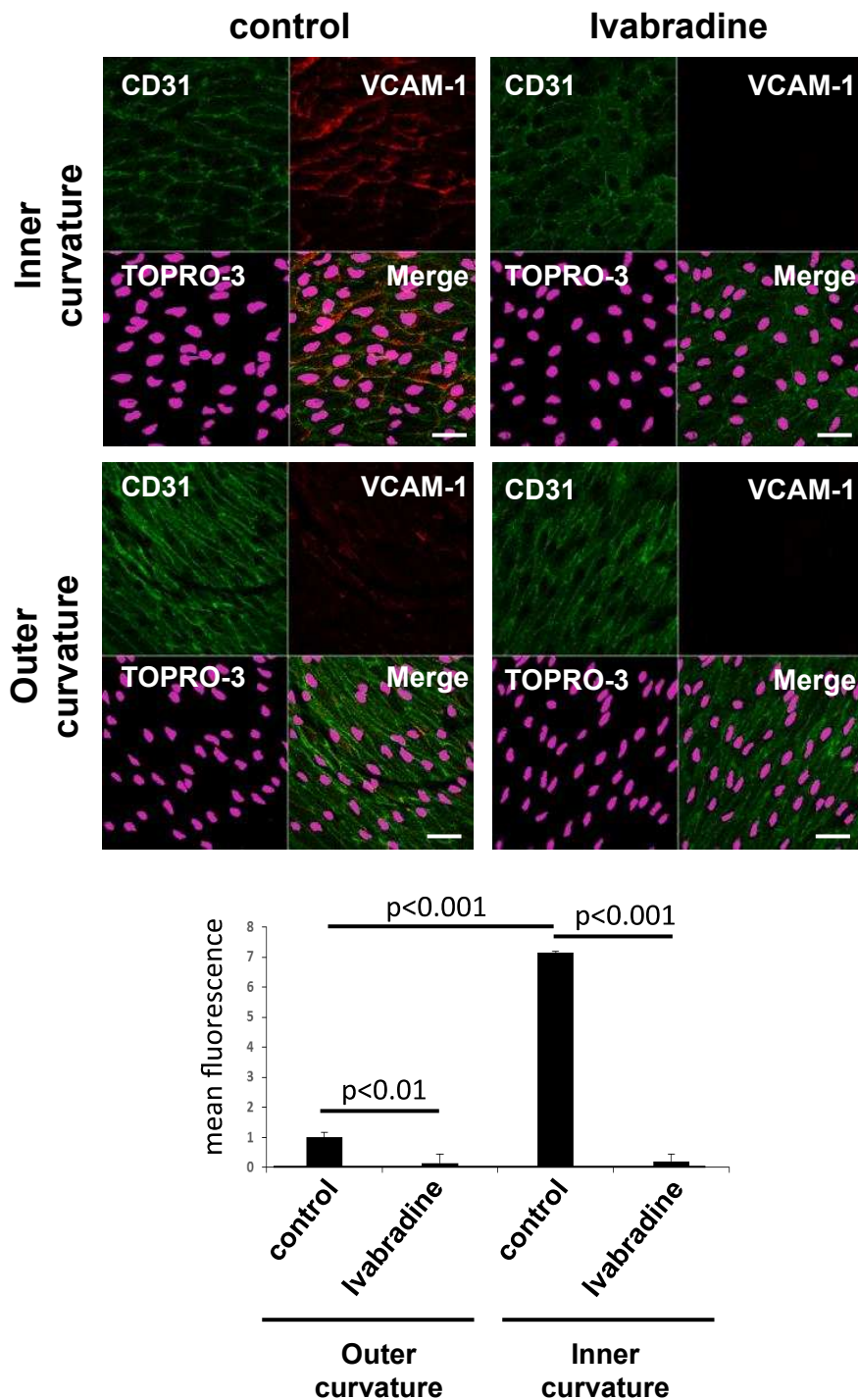
**Figure 2   Ivabradine reduced endothelial expression of VCAM-1 in the murine aorta.**

LDLR$^{-/-}$ mice aged 9 weeks were treated using ivabradine (in drinking water) or remained untreated as a control (n=5 per group). After 1 week, both groups of mice were exposed to a high fat diet in the presence or absence of ivabradine treatment. Following 6 weeks, VCAM-1 expression levels in EC were assessed by *en face* staining of the inner and outer curvatures (red). EC were identified by co-staining with anti-CD31 antibodies conjugated to FITC (green). Cell nuclei were identified using TOPRO-3 (purple). Representative images and quantitation of VCAM-1 expression (mean +/- SEM) are shown. Scale bar, 20 μm. Differences between means were analysed using a 2-way ANOVA.

Figure 3   Ivabradine induced endothelial expression of eNOS in the murine aorta. LDLR^{-/-} mice aged 9 weeks were treated using ivabradine (in drinking water) or remained untreated as a control prior to exposure to high fat diet for 6 weeks (n=7 control group, n=8 ivabradine group). eNOS expression levels in EC were assessed by *en face* staining of the inner and outer curvatures (red). EC were identified by co-staining with anti-CD31 antibodies conjugated to Alexa Fluor® 488 (green). Cell nuclei were identified using TOPRO-3 (purple). Representative images and quantitation of eNOS expression (mean +/- SEM) are shown. Scale bar, 20 μm. Differences between means were analysed using a 2-way ANOVA.
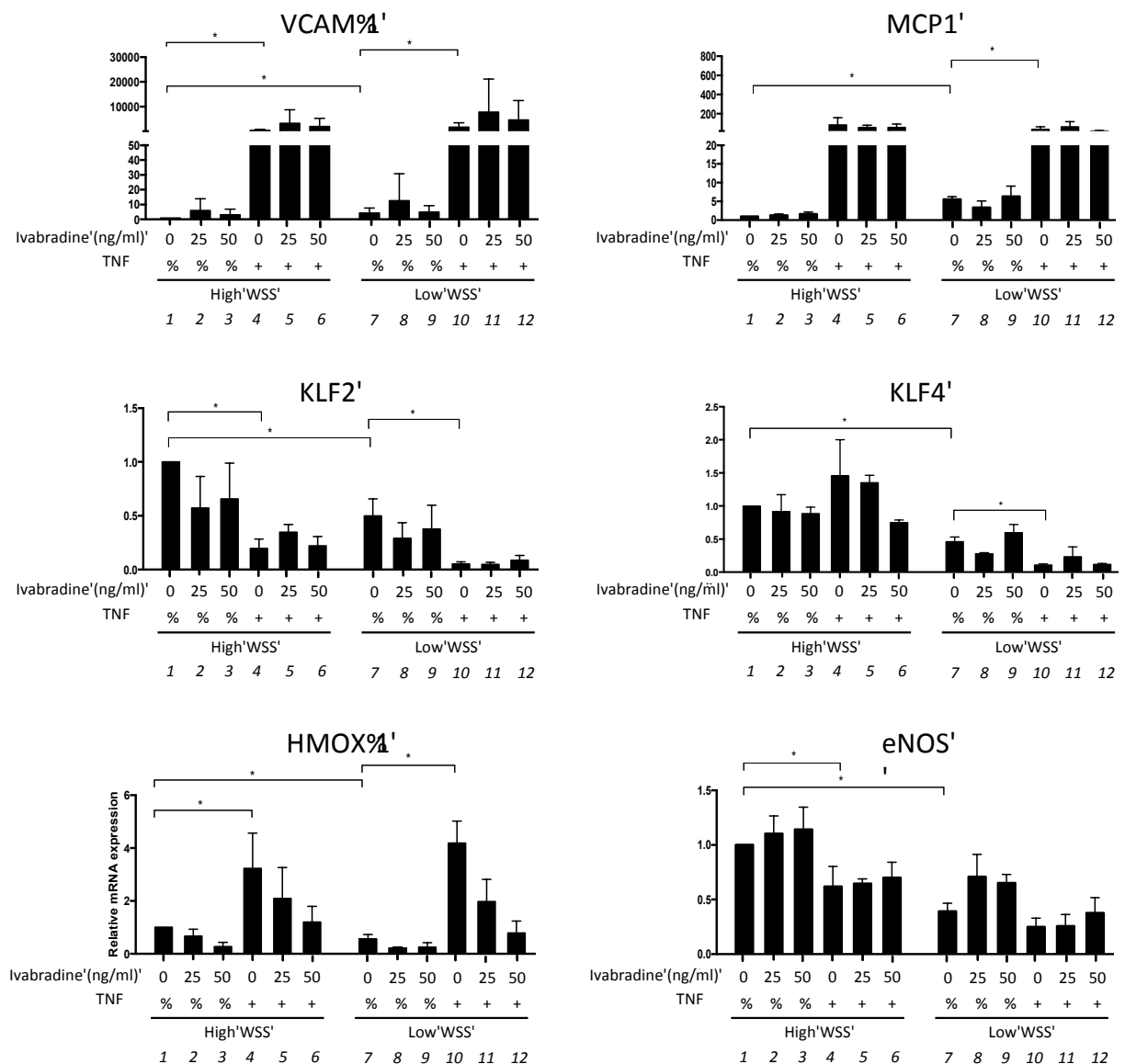
Figure 4   **Ivabradine did not regulate inflammatory or protective gene expression in cultured endothelial cells.** (A) HUVEC were exposed to low or high WSS for 72 h in the presence of varying concentrations of ivabradine (or in the absence of ivabradine as a control). Some cultures were subsequently exposed to TNFα (10 ng/ml) from 68-72 h. The expression levels of specific transcripts were measured by qRT-PCR. Data were pooled from 3 independent experiments and mean values +/- standard errors are shown. Differences between means were tested using a 2-way ANOVA. Only significant differences are indicated.
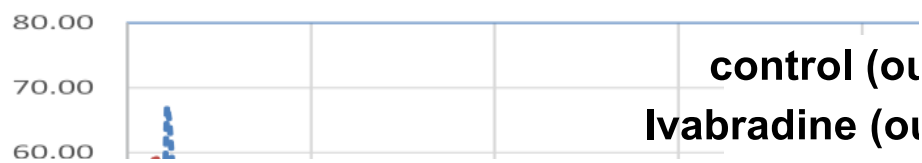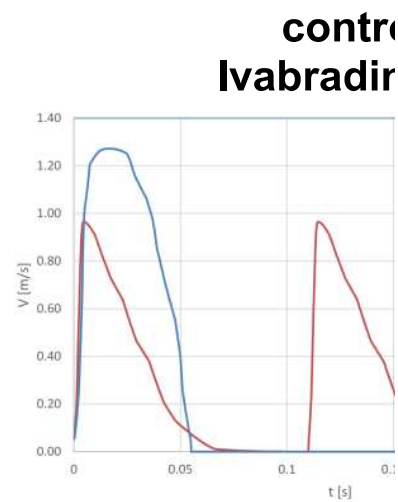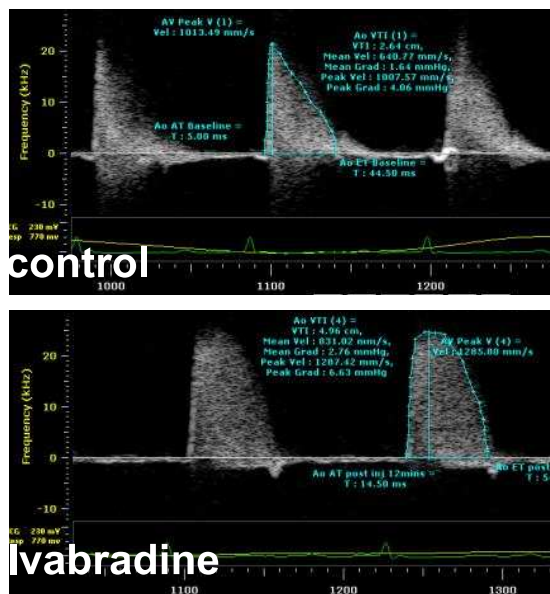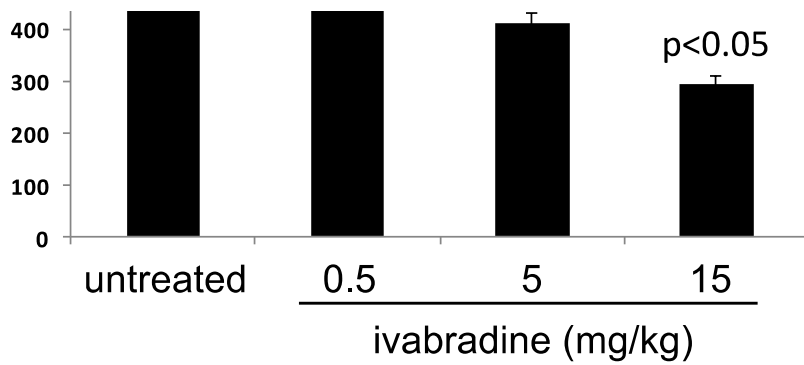
Figure 5 Ivabradine altered hemodynamics in the murine aorta. (A) LDLR$^{-/-}$ mice aged 9 weeks were sedated using isofluorane prior to assessment of baseline heart rates by transthoracic echocardiography (untreated). (A) Mice were treated with 0.5, 5 or 15 mg/kg ivabradine (i.v.) and heart rates were measured 15 min later. Data were pooled from 5 mice and mean values +/- standard deviations are presented. (B, C) LDLR$^{-/-}$ mice aged 9 weeks were sedated using isofluorane. Mice were then treated with ivabradine (5 mg/kg; i.v.) and repeat measurements of aortic blood flow were made 15 min later (ivabradine). (B) Ultrasound data (left panels) were used to generate velocity waveforms (right panels). (C) The velocity distributions were used as boundary conditions for CFD assessment of the aorta. WSS was calculated over the cardiac cycle at outer and inner curvatures of the aorta in basal (control) and ivabradine-treated conditions. Data shown are representative of those generated in 5 independent experiments.
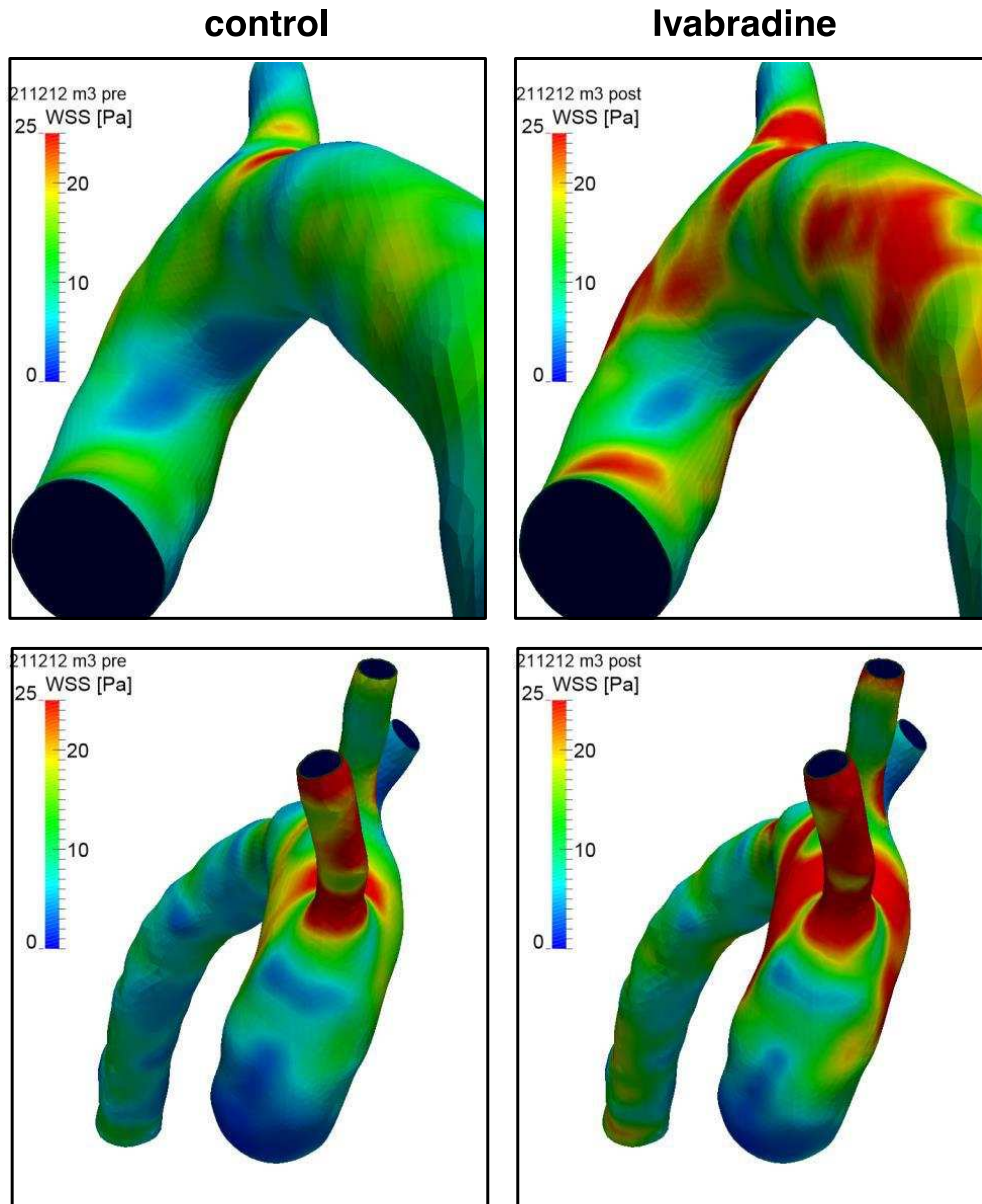
Figure 6   Ivabradine enhanced wall shear stress in the murine aorta. LDLR^{-/-} mice aged 9 weeks (n=5) were sedated prior to the assessment of blood flow velocities in the aorta either prior to (control) or following administration of ivabradine (5 mg/kg; i.v.). The velocity distributions were used as boundary conditions for CFD assessment of the aorta. Time-averaged WSS were calculated and mapped onto the aortic geometry. Representative data from 5 independent experiments are shown in two orientations (inner curvature, upper panels; greater curvature, lower panels). Note that the brachiocephalic and left common carotid arteries are hidden in the upper panels due to the orientation of the vessel.